Thermal Decomposition Properties of *Pinus radiata* Derived Polyvinyl Alcohol/Carbon Quantum Dot Composites

Shiqi Xu, Keke Liang, Zhuangzhuang Teng, and Yutong Wang

Although carbon quantum dot (CQDs) films exhibit excellent optical, mechanical, and water resistance properties, they have received less attention in terms of thermal stability. Attention to the thermal decomposition behavior is of significant importance to the heat treatment process. Different models were used to calculate the pyrolysis kinetic parameters of the films, including the Flynn-Wall-Ozawa method, the modified Coats-Redfern method, the Kissinger method, the Friedman method, and the Gaussian fitting method. The results showed that half of the mass loss of the film occurred at 300 °C, and 80% of the mass loss occurred in the next 200 °C. The apparent activation energy of the films ranged between 110 and 150 kJ/mol. The addition of CQDs and nanocellulose did not improve the apparent activation energy of the films, but it slowed down the rate of mass loss of the films. The thermal decomposition behavior is useful to understand the properties of the films during the blending, heat treatment and to guide the processes such as heat treatment.

DOI: 10.15376/biores.21.2.4872-4898

Keywords: Carbon quantum dots; Pyrolysis kinetics; Model; Apparent activation energy

Contact information: Co-Innovation Center of Efficient Processing and Utilization of Forest Products, College of Materials Science and Engineering, Nanjing Forestry University, Nanjing, 210037, China; Corresponding author: nlwyt@njfu.edu.cn

INTRODUCTION

Polyvinyl alcohol (PVOH), a linear polymer, has many excellent properties, such as being easily soluble in water and being manufactured into films (Yeum *et al.* 2004). Not only that, the mechanical properties of PVOH are also excellent (Lin *et al.* 2020). The excellent performance of PVOH makes it possible to have applications in many fields, such as the battery field (Shin *et al.* 2007), pharmaceutical field (dos Santos *et al.* 2020), and environmentally friendly materials (Zhang *et al.* 2016), *etc*. However, PVOH has certain disadvantages due to its own properties. PVOH molecular chain contains a large number of carbonyl groups; these will become unstable when encountering water, will become unstable (Limpan *et al.* 2012; Bersanetti *et al.* 2019). The thermal stability of PVOH is poor, and decomposition behavior will occur at 240 °C (Zhang *et al.* 2016). However, PVOH side groups contain a large number of hydrogen bonds between them, and these hydrogen bonds allow PVOH to react with other substances (Yeum *et al.* 2004), which changes its molecular structure.

Carbon materials, as reinforcement materials, are popular functional composites (Stankovich *et al.* 2006). Nanofibrillated cellulose, as a carbon material, is widely available (Wang *et al.* 2019). NFC can be used to enhance the performance of PVOH films because

of its high strength, stiffness, recyclability, and large surface area (Klemm *et al.* 2010; Dufresne 2013; Patchiya *et al.* 2018). *Pinus radiata* is a fast-growing tree species (Garrett *et al.* 2021), mainly from New Zealand and Australia. With its medium density, homogeneous structure, and high stability, *Pinus radiata* is widely used in construction and other applications (Tian *et al.* 2016). However, *P. radiata* has many knots, high pine resin content, and large differences in heartwood and sapwood, which limit the efficient use of *P. radiata*.

Carbon quantum dots (CQDs) are spherical carbon nanoparticles with diameters below 10 nm (Baker and Baker 2011). CQDs, a strongly fluorescent nanomaterial, was discovered in 2004 (Xu *et al.* 2004), but it was not prepared until 2006 (Sun *et al.* 2006). In addition to their excellent fluorescence characteristics (Chen and Fan, 2017), CQDs have additional advantages, such as low production costs (Wang *et al.* 2015), stable chemical properties (Guo *et al.* 2019), good photostability (Mehta *et al.* 2017), and low biological toxicity (Hao *et al.* 2021), *etc*. These excellent characteristics make CQDs an excellent alternative for many applications, such as analytical testing (Guo *et al.* 2015), bio-sensing (Li *et al.* 2010), and bioimaging (Kong *et al.* 2012).

There are many methods for the synthesis of CQDs. The arc discharge method was the first method to prepare CQDs (Xu *et al.* 2004). However, Bottini, *et al.* (2006) suggested in a later study that this method produced low yields of CQDs and, worse, unstable fluorescence properties of CQDs. Laser etching is another method of preparing CQDs, which allowed the carbon nanoparticles to be exfoliated and the carbon targeted to be etched with a laser under low temperature and high pressure (Sun *et al.* 2006). The selected voltage was applied to a working electrode of conductive carbon material and the electrolyte helped to exfoliate the carbon nanoparticles on the anodic oxide electrode, a method known as an electrochemical method (Zhou *et al.* 2007). The hydrothermal synthesis method allowed different precursors to undergo hydrothermal reactions to obtain CQDs (Zhang *et al.* 2010; Pei *et al.* 2015; Ding *et al.* 2016).

Xu *et al.* (2019) reported excellent performance of *P. radiata* derived polyvinyl alcohol/carbon quantum dot films in terms of optical, mechanical, water resistance and wetting properties. CQDs enhanced the UV-blocking properties of the films, which increased with the content of CQDs. In addition, CQDs and NFC together enhanced the mechanical properties of the films. El-Shamy (2019) similarly found an enhanced effect of CQDs on the mechanical properties of the films. The water absorption and surface contact angle of the composite films were evaluated to decrease with the increase in the content of CQDs. Some ideas are to enhance the performance of PVOH by adding specific substances to PVOH. Yang's application to piezoelectric biomaterials, which had higher tensile strength than PVOH films, provided scalable and simple solution for creating high-performance piezoelectric biomaterials for the development of transient implantable electromechanical devices (Yang *et al.* 2021). In addition, the laminated film exhibited antimicrobial and antioxidant properties that PVOH films did not. Although the research of Xu *et al.* (2019) provides a good foundation, many applications of thermoplastic polymers required them to withstand high temperatures during molding, often above 200 °C. Co-mingling (Sarma *et al.* 2018), heat treatment (Liu *et al.* 2010), and other processes to further optimize the performance of PVOH, enhance the competitiveness of PVOH products, and broaden its application range. Pyrolysis kinetic analysis is an important tool to describe the influence of process parameters on the feedstock conversion process (Cai *et al.* 2018). More importantly, the study of their thermal decomposition behavior has significant implications for processes such as heat treatment.

In this study, hydrothermal method pretreatment was applied to prepare CQDs from *Pinus radiata* wood flour in the first step. PVOH solution and NFC solution were added into CQDs and used different methods to prepare CQDs/PVOH films and CQDs/PVOH/NFC films. Thermodynamic analysis was performed by thermogravimetric analysis (TGA) and differential scanning calorimetry (DSC). The theoretical approach in this work included consideration of the F-W-O, C-R, and Kissinger models. These were used to calculate the apparent activation energy.

EXPERIMENTAL

Material Preparation

Jingjiang Guolin Forest Co., Ltd. (Jiangsu, China) provided processing residues of *Pinus radiata* wood. The wood flour was received and dried in an oven, where the temperature was set to 105 °C until the wood flour mass was constant. A pulverizer (400Y, Yongkang baao hardware products Co. Ltd., Zhejiang, China) was used to crush this wood powder. The wood flour was then screened by a 90-mesh sieve. Zhongshan Nan Fiber New Material Co., Ltd. (Guangdong, China) provided coniferous nanocellulose suspension. Its solid content, fiber diameter, and aspect ratio were 2.5±0.5 wt.%, 30 nm, and 220, respectively. Both PVOH (degree of polymerization, 750 t 50) and quinine sulfate (99.4%) were purchased from Aladdin Biochemical Co., Ltd. (Shanghai, China). All chemicals were used as received, without further purification.

Composite Preparation

CQDs were synthesized using a hydrothermal method. Purified water (70 mL) was stirred vigorously while *Pinus radiata* wood flour (1.3 g) was added. A high-pressure Teflon-lined stainless steel autoclave (100 mL, Taizhou, China) containing the mixed solution was heated for 8 h in an oil bath at 200 °C. The autoclave was then removed and cooled to room temperature. A microporous membrane (pore size of 0.22 μm) was used to filter the mixed solution from the autoclave. The mixture was dialyzed by a dialysis membrane (MWCO 500-1000 Da, Spectrum Labs, Los Angeles, CA, USA) for 48 h to obtain CQDs with a concentration of 0.1 wt.%. The formulation of *P. radiata* derived polyvinyl alcohol/carbon quantum dot composites is shown in Table 1.

The 10 wt% PVOH solution was obtained by stirring 10 g of PVOH and 90 mL of purified water at 95 °C for 2 h. The 1 wt% NFC solution was obtained from purchased NFC solution (8 g, 2.5 wt.%) and deionized water (12 mL) by vigorous stirring for 1 h at room temperature. 10 ml of PVOH solution (10 wt%) was placed in a Petri dish and subsequently heated in an electric blast oven (101-2BS, Beijing Hanoi Lixing Technology Co., Ltd., China) at 40 °C for 24 h. PVOH films were prepared and labeled as No.1.

First, 2.0 mL of CQDs solution (0.1 wt%) and 10 mL of PVOH solution (10 wt.%) were mixed and sonicated in an ice-water bath (XO-1200, Najing Xianquai Biotechnology Co., Ltd., China) at 20 to 25 kHz and 960 W output power for 30 min. The mixture was cast into a 90 mm diameter glass culture dish and heated in the oven (101-2BS, Beijing Hengnuolixing Technology Co., Ltd., China) at 60 °C until smooth delamination. The obtained CQDs/PVOH films were labeled as No.2.

Next, 4.0 mL of CQDs solution (0.1 wt.%) and 10 mL of PVOH solution (10 wt.%) were mixed in the same way and the resulting films were labeled as No.3.

PVOH solution (10 wt%) and NFC solution (1 wt%) were mixed and then sonicated

(XO-1200, Nanjing Xianke Biotechnology Co., Ltd., China) in an ice/water bath at 20 to 25 kHz for 40 min. The PVOH/NFC mixture was treated for 40 min at 20-25 kHz with an output power of 960 W to obtain. 20 mL of PVOH/NFC mixture was cast into a 90 mm diameter glass Petri dish and heated in an oven (101-2BS, Beijing Hengnuolixing Technology Co., Ltd., China) at 60 °C until the films were smoothly peeled off. The obtained films were labeled as No.4.

The films obtained after 2 mL CQDs solution (0.1 wt%) and 20 mL PVOH/NFC mixture were sonicated and heated in the same manner were labeled as No.5.

A total of 4.0 mL CQDs solution (0.1 wt%) and 20 mL PVOH/NFC mixture were sonicated and heated in the same manner were labeled as No.6.

Table 1. Formulation of *Pinus radiata* Derived Polyvinyl Alcohol/Carbon Quantum Dot Composites

No	Solution of PVOH and NFC/mL	V_{PVOH}:V_{NFC}	CQDs/ml
1	10	10:0	0
2	10	10:0	2
3	10	10:0	4
4	20	10:10	0
5	20	10:10	2
6	20	10:10	4

Thermogravimetric Analysis (TGA)

The thermogravimetric analyzer TG209F3 (Netzsch Group, Selb, Germany) was used to test the pyrolytic loss of mass loss processes. Thermogravimetric analysis of radiata pine derived polyvinyl alcohol/carbon quantum dot composites was performed to efficiently and accurately model the pyrolytic mass loss process. The temperature was set at 30 to 800 ℃ with a heating rate of 5, 10, 15, or 20 ℃/min. First the samples were dried in an oven for 24 h. The temperature of the oven was set to 70 °C. After drying, the samples were put into a thermogravimetric analyzer for testing. The protective gas in the thermogravimetric analyzer was nitrogen with a gas flow rate of 30 mL/min. Sampling segments were set every 0.5 seconds.

Differential Scanning Calorimetry (DSC)

The DSC test was used to compare the thermal behavior of the films. DSC tests were performed by a DSC 200 thermal analysis system (NETZSCH, Germany). All sample tests were performed under nitrogen protection. Prior to DSC testing, the samples were enclosed in aluminum sample trays with each sample weight strictly maintained between 4-8 mg, and then heated to 250 °C at a heating rate of 10 °C/min.

Theoretical Approach

Pyrolytic kinetic equations are based on the following basic equations,

$$\frac{d\alpha}{dt} = kf(\alpha) \quad (1)$$

where k is the rate constant and $f(\alpha)$ is the reaction model, which was determined by the reaction mechanism. Equation 1 shows the conversion rate. $d\alpha/dt$ is the rate of loss of reactant concentration. The conversion rate α is defined as,

$$\alpha = (W_0 - W_t)/(W_0 - W_f) \quad (2)$$

where W_0, W_t, and W_f are the initial, time t, and final mass of samples, respectively.

The Arrhenius equation usually defines the rate constant k like this,

$$k = A \exp(-E_a/RT) \quad (3)$$

where E_a is the apparent activation energy (kJ/mol), R is the gas constant (8.314 J/K mol), A is the pre-exponential factor (min $^{-1}$), and T is the absolute temperature (K). Bringing Eqs. 2 and 3 into Eq. 1 yields:

$$d\alpha/dt = A \exp(-E_a/RT) f(\alpha) \quad (4)$$

Introducing the heating rate $\beta = dT/dt$ into the dynamic TGA calculation method yields:

$$d\alpha/dt = (A/\beta) \exp(-E_a/RT) f(\alpha) \quad (5)$$

Under conditions of linear warming:

$$T = T_0 + \beta t \quad (6)$$

Therefore

$$d\alpha/dT = (A/\beta)\, exp(-E_a/RT) f(\alpha) \quad (7)$$

Separating the variables yields:

$$d\alpha/f(\alpha) = (A/\beta) \exp(-E_a/RT) dT \quad (8)$$

The simultaneous integration of both sides in equation (8) yields:

$$\int_0^\alpha \frac{d\alpha}{f(\alpha)} = \frac{A}{\beta} \int_{T_0}^{T} \exp\left[-\frac{E_a}{RT}\right] dT \quad (9)$$

Model fitting (Caballero *et al*. 1995) is the most widely used method, but it requires the assumption of a reaction model and trial calculations, which is computationally intensive. Compared with the traditional model fitting method, the "model free" method can be used to calculate the kinetic parameters without assuming a reaction model, and the computational effort is small.

The most common "model-free" methods used in this study are summarized in Table 2. The Friedman's method (Conesa *et al*. 1995) is an equal-transformation-rate differential method. By taking the logarithm of both sides of Eq. 7, one obtains:

$$\ln\left(\frac{d\alpha}{dt}\right) = lnA + \ln[f(\alpha)] - \frac{E_a}{RT} \quad (10)$$

When the conversion ratio is constant, the value of the mechanism function $f(\alpha)$ must be constant, so that $\ln(d\alpha/dt)$ is proportional to $1/T$.

The Flynn-Wall-Ozawa method (Ozawa and Takeo 1965; Flynn and Wall 1966) is an isoconversion integration method. Taking the logarithm of both sides of Eq. 9,

$$lg \int_0^\alpha \frac{d\alpha}{f(\alpha)} = lg \frac{AE_a}{R} - lg\beta + lg \frac{E_a}{RT} \quad (11)$$

Make

$$u = \frac{E_a}{RT} \quad (12)$$

$$\frac{A}{\beta} \int_{T_0}^{T} \exp\left(\frac{E_a}{RT}\right) dT = \frac{AE_a}{\beta R} p(u) \quad (13)$$

$$p(u) = \frac{\exp(-u)}{u^2}(1 - \frac{2!}{u} + \frac{3!}{u^2} - \frac{4!}{u^3} + \cdots) \quad (14)$$

Substituting the approximate value of Eq. 14 into Eq. 9 produces Eq. 15.

$$lg\beta = \lg\left[\frac{AE_a}{R\int_0^{\alpha}\frac{d\alpha}{f(\alpha)}}\right] - 2.315 - 0.4567\frac{E_a}{RT} \quad (15)$$

As shown in Eq. 9, when the conversion rate α is assumed to be a constant, the mechanism function $f(\alpha)$ must also be a constant, so $lg\beta$ is proportional to $1/T$.

Table 2. Summarizing the Kinetic Methods Used for the Activation Energy Assessment

Method	Expression	Plots	References
Flynn-Wall-Ozawa	$\lg\beta = \frac{\lg(AE_a)}{Rf(a)} - 2.315 - \frac{0.4567E_a}{RT}$	$\lg\beta$ *vs.* $\frac{1}{T}$	Ozawa and Takeo (1965); Flynn and Wall (1966)
Coats-Redfern (modified)	$\ln\left[\frac{\beta}{T^2\left(1-2\frac{RT}{E_a}\right)}\right] = \ln\left[\frac{AR\left(1-\frac{2RT}{Ea}\right)}{\beta E_a}\right] - \frac{E_a}{RT}$	$\ln\left(\frac{\beta}{T^2}\right)$ *vs.* $\frac{1}{T}$	Brown *et al*. (2000)
Friedman	$\ln\left(\frac{d\alpha}{dt}\right) = \ln[Af(\alpha)] - \frac{E_a}{RT}$	$\ln\left(\frac{d\alpha}{dt}\right)$ *vs.* $\frac{1}{T}$	Friedman (1964)
Kissinger	$\ln\left(\frac{\beta}{T_P^2}\right) = \ln\left(\frac{AR}{E_a}\right) + \left(\frac{1}{T_P}\right)\left(-\frac{E_a}{R}\right)$	$\ln\left(\frac{\beta}{T_P^2}\right)$ *vs.* $\frac{1}{T_P}$	Kissinger (1956)

The modified Coats-Redfern method (Marini *et.al*. 1979) is a multi-heating rate application of the Coats-Redfern equation. Plotting the left-hand side for each heating rate versus $1/T$ at that heating rate gives a family of straight lines of slope $-E_a/R$. The full solution is to be done iteratively by first assuming a value of E_a and then recalculating the left-hand side until convergence occurs. Here, a quick solution, however, is also available by moving $(1 - 2RT/Ea)$ into the intercept and assuming that it is a constant.

$$\frac{d\alpha}{dt} = \beta\frac{d\alpha}{dT} = (1-\alpha)^n Ae^{\frac{-E_a}{RT}} \quad (16)$$

According to the Kissinger method (Kissinger 1956), when the thermal analysis curve has an extreme value, $T = Tp$, $d(d\alpha/dt)/dt = 0$, one derives the derivative of Eq. 16 on both sides and brings the boundary conditions to obtain:

$$\ln\left(\frac{\beta_i}{T_{pi}^2}\right) = \ln\left(\frac{AR}{E_a}\right) + (\frac{1}{T_{pi}})(-\frac{E_a}{R}) \quad (17)$$

Data processing

The data obtained from the experiment were processed and analyzed using EXCEL 2016, ORIGIN 2018, PHOTOSHOP 2019, and GRAPHPAD PRISIN 5 software. The experimental design was considered to be reasonable if the mass loss curves obtained from two separate experiments on the same sample under the same experimental conditions were approximated (Brown *et al.* 2000).

RESULTS AND DISCUSSION

Overall Decomposition Process

The TGA curves and DTG curves obtained by testing the films are collated in Fig. 1. The TGA and DTG curves at 5, 10, 15 and 20 °C/min were very similar. However, the TGA and DTG curves at the heating rate of 5°C/min contained more details because the smaller heating rate allowed for more time for mass changes to occur.

The mass loss curves of the pure PVOH films followed the same trend as those of the films with CQDs and NFC added. The curves of each sample overlapped after 230 °C. However, from 30 to 230 °C, the mass loss of pure PVOH film was greater than that of the other samples. This phenomenon is demonstrated in Fig. 1(a), *i.e*., the TG curve of pure PVOH film was lower than that of the other samples. A small change in mass loss rate occurred at 102 °C, and this phenomenon is shown in Fig. 1(b) and marked with arrows. In fact, 30 to 230 °C was considered to be the first stage of PVOH pyrolysis (Tang and Alavi 2011; Voronova *et al.* 2015).

The mass loss in this process was mainly caused by the evaporation of the adsorbed water. The mass loss of the pure PVOH film reached 10%. However, the other samples only lost 5% of their mass at a temperature of 102 °C. This phenomenon can explain why the addition of CQD and NFC can improve the thermal stability of PVOH films from 30 to 230 °C. In other words, films with more hydrogen bonds are more likely to bind to NFCs or CQDs, and breaking these bonds requires additional energy. The second stage occurred at 230 to 390 °C, which was also the most important stage of PVOH mass loss (Lu *et al.* 2008).

In this study, PVOH reached its maximum mass loss rate at 276 °C, at which point it lost 39% of its mass. The film lost 83% of its mass when the temperature came to the end of the second stage, *i.e.* 390 °C. The degradation of PVOH starts in the second region, mainly involving hydroxyl dehydration and the formation of volatile organic compounds and conjugated, unsaturated polyenes (Sin *et al.* 2011). The third stage was defined as the temperature exceeding 390 °C. In this study, the third stage temperature range was defined as 390 to 800 °C. It is noteworthy that the maximum stage III mass loss rate occurred at 420 °C, which is caused by the degradation of polyene residues to olefins and alkanes as well as aromatics through intramolecular cyclization (Sin *et al.* 2011).

PVOH/CQDs films and PVOH/CQDs/NFC films underwent a mass loss process similar to that of pure PVOH films, and the mass loss process was divided into three stages. In the first stage, in particular, the mass loss curves of the films largely overlapped, except for the pure PVOH film. The composite films started thermal decomposition at the same temperature as the pure PVOH films and exhibited the maximum mass loss rate at the same temperature, and there was no consistent trend with increasing content of NFC and CQDs. This phenomenon showed that NFC and CQDs did not significantly improve the thermal stability of PVOH. Although the mass loss curves of different films had the same trend, there was still a phenomenon worth noting. PVOH films without the addition of NFC and CQDs degraded at 30 to 230 °C with a maximum mass loss of 11.5%. However, PVOH films with the addition of NFC and CQDs had a mass loss of 6.3 to 7.1% at 30 to 230 °C. PVOH-based polymeric films are sometimes used for melt processing, so the addition of NFC and CQDs can expand their melt processing window (Zhang *et al.* 2014).

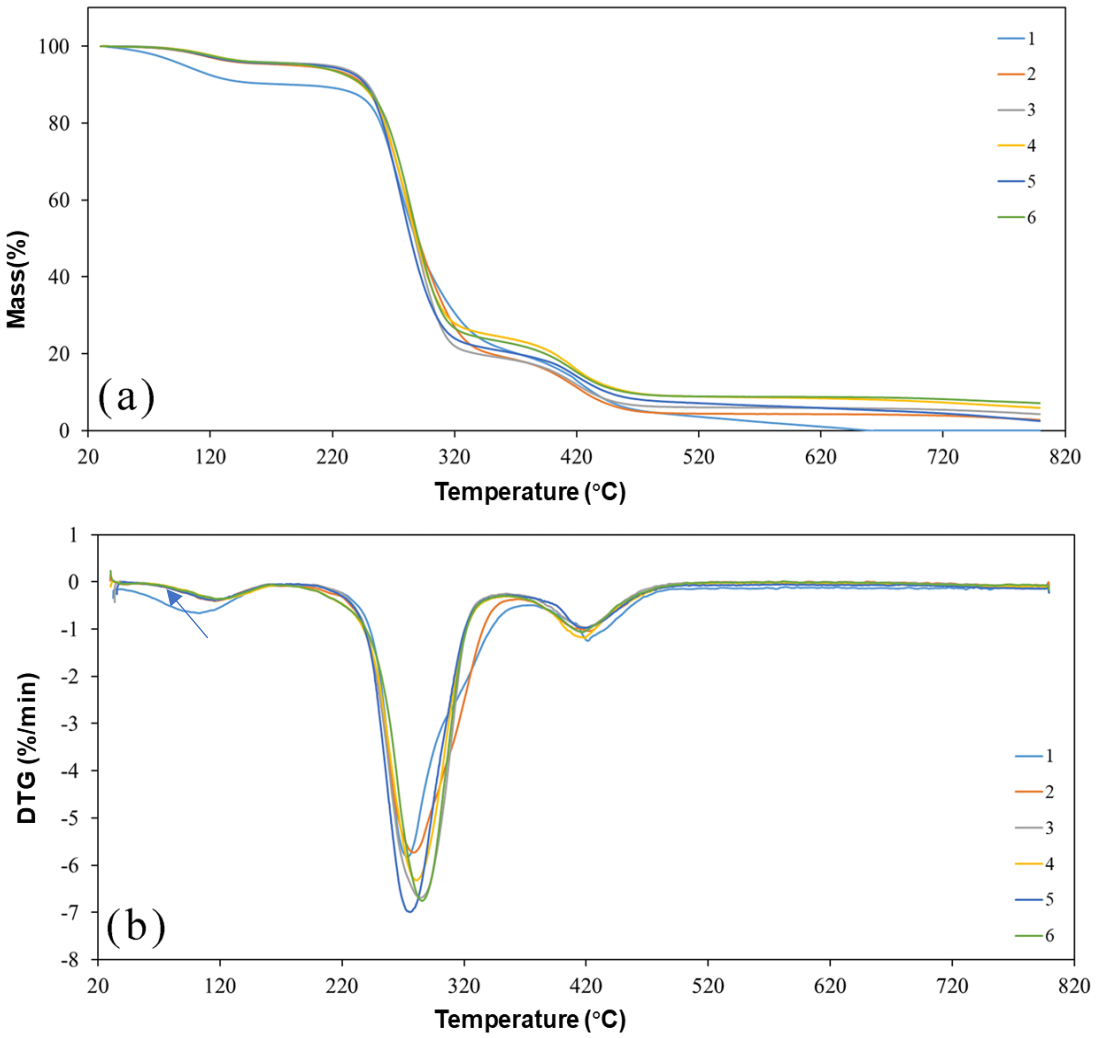

Fig. 1. Thermal analysis of the film (a) TGA and (b) DTG

The addition of NFC accelerates the rate of mass loss, as more mass remains in the pure PVOH film at the same temperature in the range of 290 to 375 °C. The residual mass of the pure PVOH film reached 48% at 290 °C, while the residual mass of sample No.5 at this temperature was only 42%. NFC failed to produce a film with much higher thermal stability than pure PVOH, which was confusing because NFC was much more thermally stable than PVOH (Takahashi *et al.* 2014; Wang *et al.* 2020). NFC left traces in the DTG curve during thermal decomposition; the peaks appearing at 235 °C correspond to the degradation of carboxylated surface chains, and the peaks appearing at 283 °C correspond to the degradation of unmodified crystalline nuclei (Jiang and Hsieh 2016). In the present study, no traces of NFC were found in these two feature temperatures. Two possible explanations are: (1) NFC and PVOH were not combined, but the amount of NFC was so small that it could not be detected by the thermogravimetric analyzer. (2) The solution binded NFC and PVOH together, which may allow NFC to react with PVOH, a slow reaction process. Both of these possible behaviors might prevent the appearance of a significant NFC peak. This phenomenon was also reported in previous studies (Voronova *et al.* 2015). These authors pointed out that NFC can improve the thermal stability of PVOH but the NFC concentration must reach a certain value. This is because the higher

concentration of NFC forms a strong network by self- entanglement through hydrogen bonding, and in addition to that, the polymer enters the cellulose structure and surrounds the cellulose filler (Lu *et al.* 2008). This behavior undoubtedly enhanced the mechanical properties and thermal stability of the composites. However, it has also been pointed out that NFC does not improve the thermal stability of the composites (Qua *et al.* 2009; Li *et al.* 2012; Silverio *et al.* 2013). The film fabrication process is considered to be the main influencing factor. Film casting on an uneven surface, as in the present study fabrication process, may amplify the difference in thermal stability of the film because of the demanding horizontal surface requirements for particle alignment (Mashkour *et al.* 2014). The particle distribution on the film is determined by the joint distribution of PVOH and NFC. If the nanoparticles are not uniformly distributed in the film, then this inhomogeneity is found in the actual filler and eventually affects the thermal stability of the film.

Table 3 summarizes the decomposition properties of the selected films. A simple approach was that the temperature at a 5% mass loss can be considered as the initial decomposition temperature (Yao *et al.* 2008). The parameter T_o indicated that the initial decomposition temperature of all films ranged from 120 to 210 °C. The parameter T_p indicated that the maximum decomposition rate of the films occurred in the range of 282 to 304 °C. Compared to the maximum temperature difference of 90 °C for the initial decomposition temperature, the maximum temperature difference of 22 °C for T_p had a smaller difference. Because PVOH was the main component of the film, the addition of NFC and CQDs improved the initial decomposition temperature, but it did not determine the temperature at the maximum decomposition rate.

The TG, DTG curve of the film during thermal decomposition determined the thermal decomposition parameters. The mass loss of pure PVOH films reaching the maximum decomposition rate was the smallest at 31.9%, which was ahead of the films incorporating other elements. Considering that the temperature corresponding to the maximum decomposition rate of all the remaining films was greater than that of the pure PVOH films, it was reasonable that their mass loss is greater. Most films had almost completed a 40% quality loss at 300±5°C, or even higher. The difference in mass loss between the offset temperature and the offset temperature indicated that for most films, 40% of the mass loss occurred in the range of approximately 100 °C. In particular, the pure PVOH film had the smallest quality loss in a larger excursion temperature range. CQDs had the capacity for improving the initial decomposition temperature and offset temperature, as can NFCs. This is because CQDs and NFC have better thermal stability. Considering that CQDs and NFCs will be used in more materials in the future, it is necessary and meaningful to examine the activation energy of the films enhanced by them.

Table 3. Decomposition Characteristics of Selected Films, Including Initial Decomposition Temperature, and Displacement Temperature, Mass Loss and Displacement Mass Loss

Sample	T_o[a] (°C)	WL_o (%)	T_p (°C)	WL_p (%)	T_o-T_p (°C)	WI_o-WL_p (%)
No.1	120.02[b]	5	282.42	31.88	162.40	26.88
No.2	192.65	5	296.53	37.13	103.88	32.13
No.3	194.74	5	299.35	45.40	104.60	40.40
No.4	205.70	5	300.51	41.14	94.81	36.14
No.5	210.30	5	295.43	40.98	85.13	35.98
No.6	186.58	5	304.45	44.97	117.87	39.97

[a] Capital: *T* = temperature, WL = mass loss; subscript: o = onset, p = DTG peak
[b] Values from four heating rates with mean value

Influence of the Heating Rate on the Thermal Decomposition Process

The TG curves of films 1, 3, and 6 at different heating rates were compiled in Fig. 2 in order to investigate the effect of heating rate on thermal decomposition. 10 °C/min was a special heating rate. Pure PVOH film, at 310 °C, at 5°C/min always remained inferior because the film treated at 5°C/min had the smallest remaining mass at the same temperature.

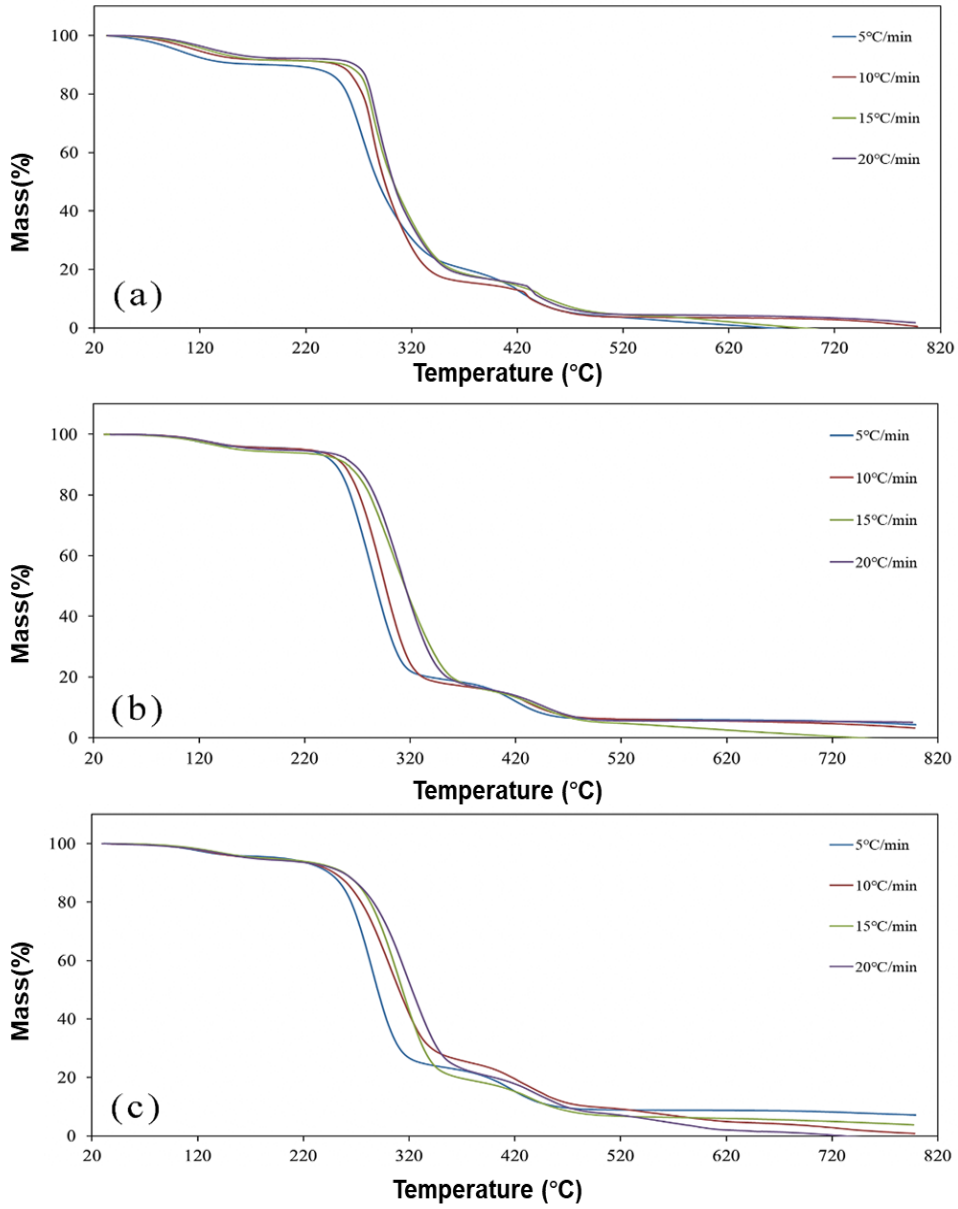

Fig. 2. TG curves of films at different heating rates, (a) film No.1. (b) film No.3. (c) film No. 6

As previously described, 230 to 390 °C was the main thermal decomposition stage of PVOH films. The mass loss of pure PVOH film reached 70% in the range of 230 to 390 °C. Thomas *et al.* (2001) reported that the strength of both carbonyl and hydrocarbon stretching modes decreases sharply starting at 220 °C, reaching a maximum rate at about 240 °C. In the range of 230 to 240 °C, the average mass loss of pure PVOH films at

different heating rates reached 1.1%. However, the average mass loss of No.2 to No.6 films at different heating rates in the range of 230 to 240 °C was 0.9%, 0.8%, 0.8%, 0.7% and 0.7%, respectively. The study of the pyrolysis mechanism of PVOH by Koverzanova *et al.* (2019) may help to explain this phenomenon. The main pyrolysis products obtained from the thermal decomposition of PVOH were used to speculate on the mechanism of PVOH pyrolysis, *i.e*., the formation of polyene structures, cyclization, and cleavage of C-C, C-H, C-O bonds and other reactions occurring simultaneously. The blending of CQDs and NFC slowed down these reactions because NFC and CQDs had hydrogen-containing groups that bind to PVOH and slowly resist thermal decomposition.

The heating rate of 10 °C/min was a special feature because of the different properties in the films with different ratios. The turning point occurred around 320 °C. By comparing the TG curves in Fig. 2 (a) and (b), the blending of CQDs made the film pyrolysis properties more similar to those of pure PVOH films. However, the blending of NFC changed this trend. Figure 2(c) showed the pyrolysis curves of PVOH/NFC/CQDs films at different heating rates. Until 320 °C, film No. 6 treated at 10 °C/min maintained a large mass loss rate, at which point the residual mass was 42%. At 320 °C, 5, 15 and 20 °C/min corresponded to a residual mass of 57%, 49% and 52%, respectively. But this phenomenon changed when the temperature range came to 320 to 520 °C. Film No. 6 treated at 10 °C/min maintained a low mass loss rate. Film No. 6 treated at 10 °C/min lost a total of 32.5% of mass at 320 to 520 °C, while 15 °C/min and 20 °C/min corresponded to a mass loss of 36.2% and 45.1%, respectively. In other words, 320 to 520 °C, and treating the films at 10 °C/min ensured maximum film integrity. A possible explanation is that a slower heating rate (<10 °C/min) and a faster heating rate (>10 °C/min) hardly accelerate the dehydration process. The elimination of water molecules is considered to be stochastic and this process can occur in any part of the molecule and is accompanied by the formation of double bonds. Not only that, it has also been suggested that the melting of PVOH microcrystals inhibits the degradation process because the heat-absorbing nature of melting may reduce the temperature of the polymer and thus the degradation rate (Thomas *et al.* 2001).

To understand the heat absorption of the films during the thermal decomposition behavior, the films were subjected to DSC tests. The DSC curves were collapsed in Fig. 3. From 30 to 150 °C, a heat absorption peak was observed for films No. 1, No. 3, and No. 6. This was a heat absorption peak due to the evaporation of water. Film No.1 absorbed more heat than films No. 3 and No. 6.

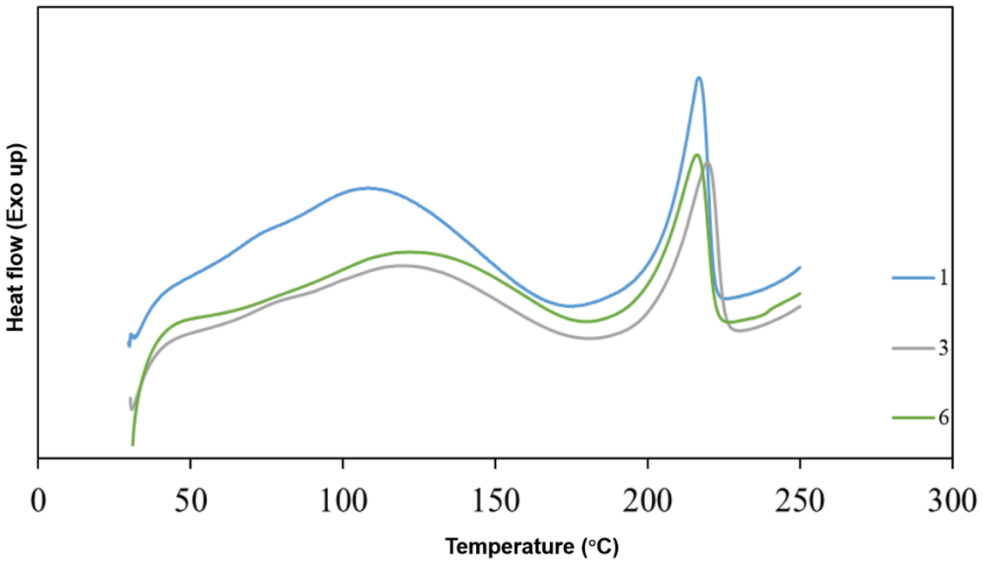

Fig. 3. DSC curves of films

No. 1, No. 3, and No. 6 films showed a clear peak of heat absorption near 220 °C. However, the peak position of No. 3 film was slightly shifted. One possible reason for this phenomenon is that the addition of NFC changes the crystal molecular weight and size distribution of PVOH. In general, the main pyrolytic behavior of cellulose in the range of 150 to 300 °C included the reduction of polymerization, formation of free radicals, inter- or intra-molecular dehydration, formation of CO_2 and CO, *etc*. After a series of reactions, the cellulose undergoes cross-linking reactions and then forms coke. In this temperature range, cellulose was converted into active fibers and the length of cellulose microcrystals is changed (Shafizadeh 1982, 1985; Evans and Milne 1987). Morán *et al.* (2008) pointed that the shift of the peak position was related to the active fiber content and the change of the fiber microcrystal length.

The addition of CQDs, as in the case of the No. 6 film curve, reduced the peak position. no additional heat absorption peaks were observed for the No. 3 and No. 6 films. However, the heat absorbed by films 3 and 6 was less than that of the pure PVOH film.

Pyrolysis Kinetic Analysis of Different Materials

Considering the introduction of NFCs and CQDs into PVOH to enhance PVOH properties, more materials may be applied in the future to enhance PVOH properties and the need to quantify the film decomposition activation energy. The F-W-O method, modified Coats-Redfern method, Friedman method, and Kissinger method were used to calculate the apparent activation energy of the films. Film No.4 was used as an example, and the process of calculating the apparent activation energy by different methods is in Fig. 4.

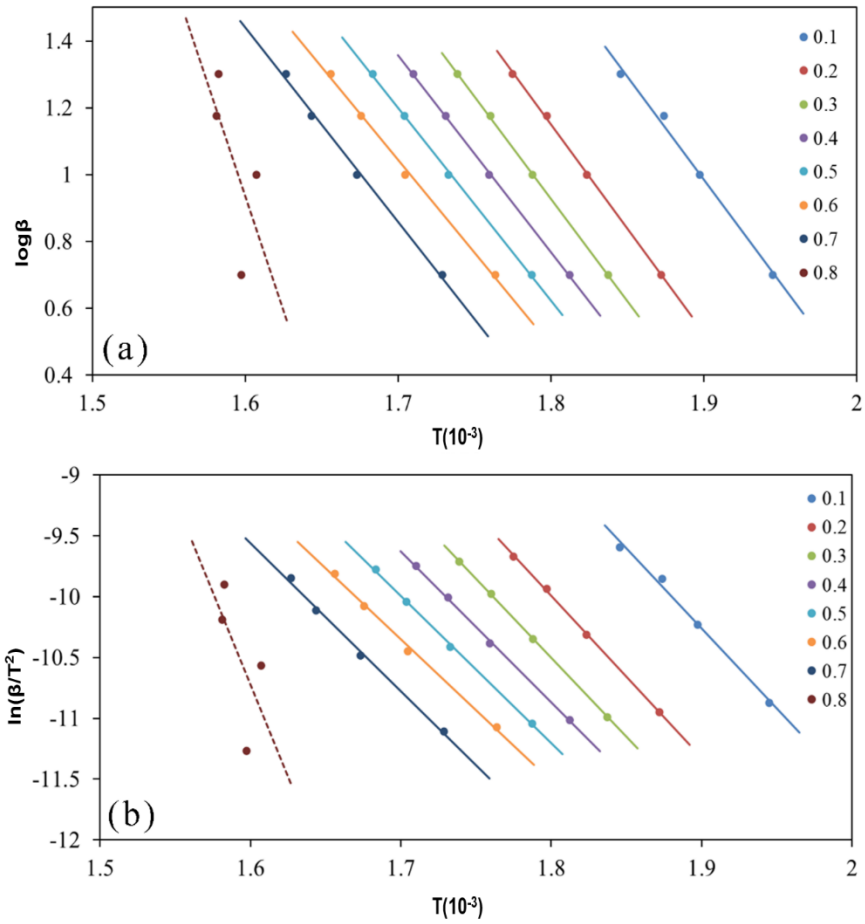

Fig. 4. Typical iso-conversional plot of (a) F-W-O method, (b) modified Coats-Redfern method

Figures 4 (a) and (b) showed that the fitted lines were almost parallel, which demonstrated the approximate apparent activation energy at different conversion rates. In fact, the parallel fitted lines can also be considered as a unification of the reaction mechanism (Yao *et al*. 2008). However, the fit was disappointing when the conversion rate reached 0.8. A possible speculation is that the response mechanism may change at higher conversion rates (usually 0.7 or higher), a condition that often occurs (Antal *et al*. 1998). In fact, a temperature range of 200 to 320 °C and a major thermal decomposition fraction of 60% are more relevant for polymer composites. Considering that the pyrolysis mechanism changes at high conversions, it would be more reasonable to focus the study on the conversion range of 0.1 to 0.7 rather than the whole process. This may provide a simplified and more meaningful method for simulating the thermal decomposition behavior of composite films.

Table 4 summarizes the average apparent activation energies of all selected films calculated by the F-W-O method, modified Coats-Redfern method, and Friedman method for conversions ranging from 0.1 to 0.7. The apparent activation energies calculated by the Kissinger method are also collated in Table 4.

Table 4. Average Apparent Activation Energy of Select Film Calculated by Three Model-Free Methods in a Period of A=0.1-0.7

No.	F-W-O		modified C-R		Friedman		Kissinger	
	E_a	R^2	E_a	R^2	E_a	R^2	E_a	R^2
1	149.3(7.3)[a]	0.9778	147.7(7.6)	0.9812	39.6	0.6399	243.5(2.8)	0.9195
2	110.8(1.3)	0.9932	107.1(1.4)	0.9922	14.6	0.5498	110.4(9.4)	0.9262
3	119.3(2.9)	0.9866	104.4(3.1)	0.9878	34.3	0.3615	116.7(1.5)	0.9883
4	108.2(4.2)	0.9994	104.4(4.7)	0.9993	23.9	0.8823	116.7(12.1	0.9975
5	119.1(12.7)	0.9941	115.9(13.6)	0.9933	24.6	0.1783	119.9(6.1)	0.9065
6	122.4(2.7)	0.9787	119.4(2.5)	0.9764	33.3	0.7317	123.4(9.7)	0.9998

a: Values from 18 conversion fractions with mean value and standard deviation

In the conversion range, the apparent activation energy calculated by the F-W-O method was in the range of 108 to 149 kJ/mol, and the calculated results were close to those reported by others (Cui *et al*. 2019). This observation was supported by similar results from the Modified C-R method and Kissinger, where the apparent activation energies of these films range from 104 to 147 kJ/mol and 110 to 243 kJ/mol, respectively. However, the apparent activation energies calculated by the Friedman method differed significantly from those calculated by the other three methods, which means that the Friedman method is not applicable to calculate the apparent activation energies of thin films. What is consistent is that the higher the content of CQDs, the higher the apparent activation energy and the higher the content of NFC, the higher the apparent activation energy. Unfortunately, the apparent activation energy of pure PVOH films always remained maximum. This conclusion was confirmed by the apparent activation energy calculated by the Kissinger method. Unlike the other three methods, the Kissinger method only used data from specific conversions to calculate the apparent activation energy, and the fit was greater than 0.91. In addition, the difference between the apparent activation energy calculated by the Kissinger method and the F-W-O and modified C-R methods was not significant. It follows that the Kissinger method is useful for determining the apparent activation energy in this case. The Kissinger method is therefore meaningful for determining the apparent activation energy in this case.

Figure 5 shows a plot of apparent activation energy versus 0.1 to 0.7 conversion rate for all films based on conversion rate methods such as F-W-O and modified C-R. The calculated apparent activation energy distribution was also clearly shown in Fig. 5.

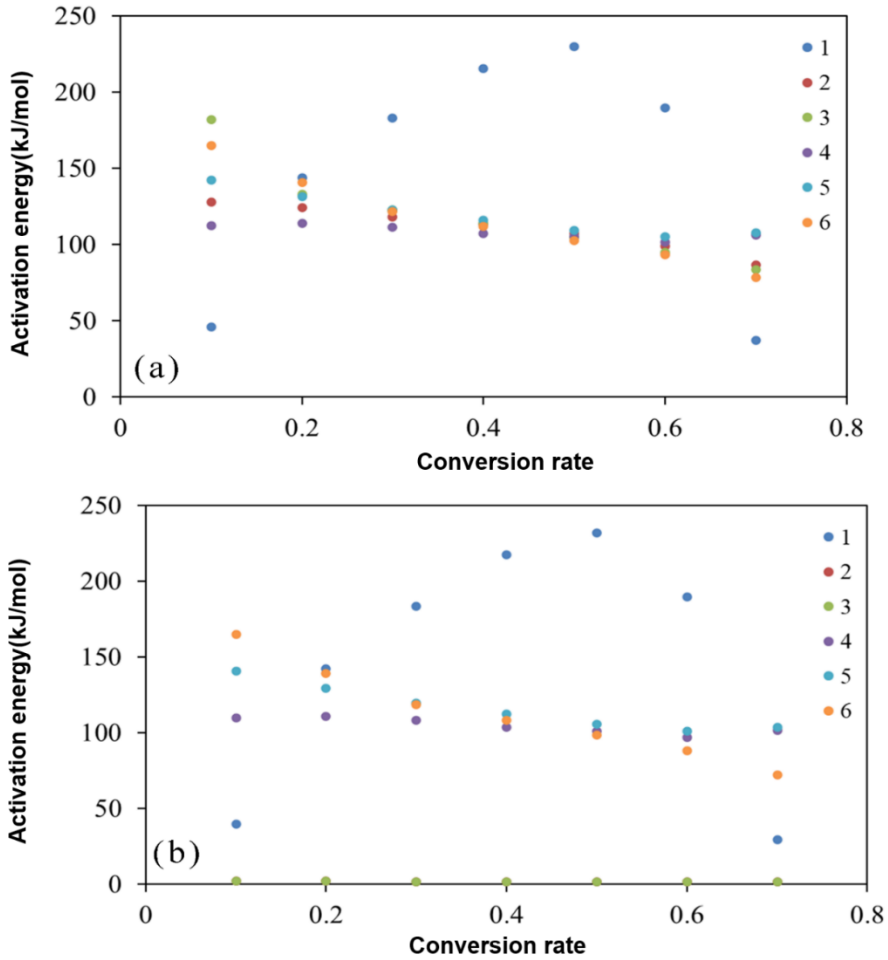

Fig. 5. A comparison of apparent activation energy as a function of decomposition conversion rate for all selected films calculated by (a) F-W-O, (b) modified C-R

As the thermal decomposition process proceeded in the films, the apparent activation energy distribution was more dispersed in the initial stage (α = 0.1), and then the apparent activation energy distributions of different films started to aggregate until α = 0.6. The dispersed behavior of the apparent activation energy at α = 0.1 indicates that the main component may undergo an accelerated decomposition process, approaching equilibrium in the initial stage. It is important to note that this dispersion behavior is different from that of α = 0.7 because the variation at high conversion rates suggests a multi-step reaction mechanism. In addition, the dispersion of pure PVOH films at different conversion rates at the apparent activation energy was the largest, which is due to different decomposition mechanisms throughout the PVOH pyrolysis process (Cui *et al.* 2019). Unlike the dispersed distribution of apparent activation energy of pure PVOH films, the apparent activation energy distribution of films incorporating NFC and CQDs was more aggregated, suggesting that the degradation mechanism (or unification of multiple reaction mechanisms) of these films is consistent across the selected conversion rate range and can be attributed to the lower temperature. In contrast, the distribution trend of the apparent activation energy of the modified C-R method, although showing a trend consistent with that of the F-W-O method, is not always accurate when calculating the apparent activation energy of the films. Some apparent activation energies were calculated as negative numbers. These apparent activation energies are not labeled in Fig. 5(b) because negative values of apparent

activation energy are not possible. The particular computational scenario that emerges implies that the thermal decomposition process of the film does not follow the modified C-R method at a certain conversion rate. In other words, the apparent activation energy calculated by the Modified C-R method may not be accurate, but it still confirms the apparent activation energy values calculated by the F-W-O method and is therefore relevant.

The different kinetic methods cooperate, not compete, with each other. The "model-free" approach does not take into account the specific reaction mechanism of the sample, which is an unavoidable error. In fact, even though the thermal decomposition behavior of the main components of the film may follow certain rules of thermal decomposition reactions with certain apparent activation energies, the complexity of the polymer leads to differences in the content. These can include, for instance, crystal structure or chemical composition of the different components. These variations are continuously changing during the thermal decomposition process. The apparent activation energies obtained in this study help to understand the range of apparent activation energies of PVOH/CQDs/NFC composite films. The apparent activation energy has the ability to imply the critical energy required to initiate the reaction.

Gaussian Model Analysis

To overcome the shortcomings of the "model-free" method, which cannot take into account the mechanism of the thermal decomposition reaction of thin films, the Gaussian multi-peak fitting method was used to calculate the apparent activation energy of thin films, referring to the prefactor A and the number of reaction steps n. The Gaussian multi-peak fitting approach assumes that the thermal decomposition mechanism employs a large number of independent, parallel, one- or multi-stage reactions that have different apparent activation energies and can respond to changes in bond strength of the substance. Apparent activation energies calculated by Gaussian multi-peak fitting methods have the ability to better understand the specific steps of the film during the thermal decomposition reaction. Preliminary kinetic parameters of the decomposition process were estimated and the process was based on experimental parameters attached to the rate profile.

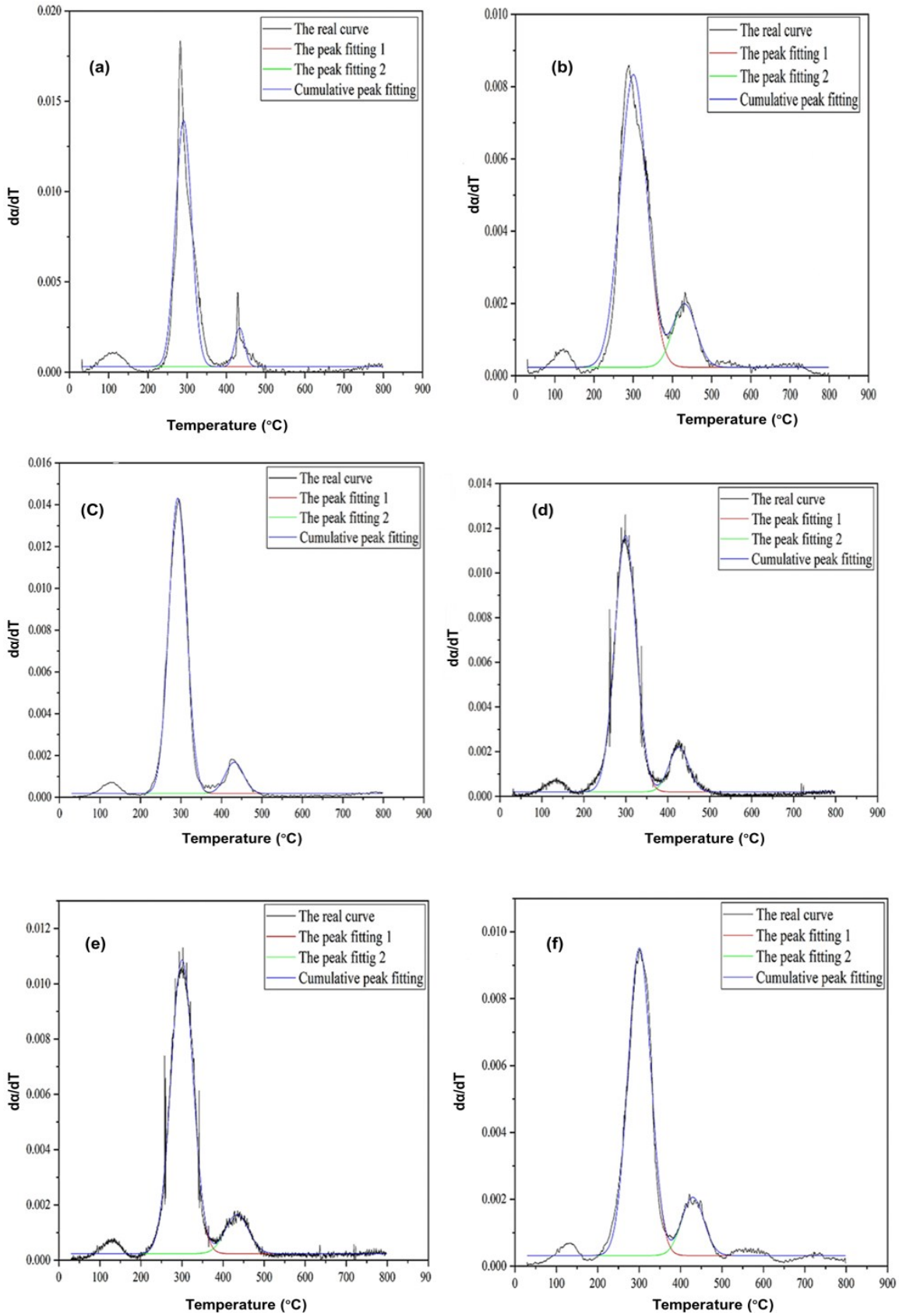

Fig. 6. Gaussian multi-peak fit. (a) film No. 1. (b) film No. 2. (c) film No. 3. (d) film No. 4. (e) film No. 5. (f) film No. 6.

Gaussian multi-peak fitting methods have been shown to be successful in separating and analyzing overlapping peaks, which typically appear on the derivative thermogravimetric (DTG) curves of sample pyrolysis. The procedure presented in this work may provide a reference for similar kinetic problems.

The DTG curves at a heating rate of 10 °C/min were simulated were shown in Fig. 6. The Gaussian peak fitting method was used for films. The Gaussian multi-peak fitting method can fit the DTG curves corresponding to different peaks. From this, the main two peaks were selected for fitting. The results calculated using the Gaussian function were in better agreement with the peak curve of film No.4, where R^2 reached 0.99.

The reaction kinetic parameters were calculated using the Arrhenius formula:

$$\frac{d\alpha_i}{dT^2} = \frac{A}{\beta}\exp\left(-\frac{E}{RT}\right)(1-\alpha_i)^2 \quad (18)$$

where $d\alpha_i/dT$ is the reaction rate of phase I (%/°C), A is the prefactor (min^{-1}), β is heating rate (°C/min), E is the activation energy (kJ/mol), R is the gas constant (kJ/(mol·°C)), T is the absolute temperature (K), and n is the number of reaction stages.

Differentiation of both sides of Eq. 18 simultaneously against T yields:

$$\frac{d^2\alpha_i}{dT^2} = \frac{A}{\beta}\exp\left(-\frac{E}{RT}\right)\left[\frac{E}{RT^2}(1-\alpha_i)^n - n(1-\alpha_i)^{n-1}\frac{d\alpha_i}{dT}\right. \quad (19)$$

Setting $T = T_c$ yields:

$$E = \frac{nH_cRT^2}{1-\alpha_i} \quad (20)$$

According to the semi-peak definition:

$$\frac{1}{2}H_c = H_c \quad (21)$$

Bringing equation 19 into equation 21:

$$\frac{1}{2}H_c = \frac{A}{\beta}\exp\left(-\frac{E}{RT_w}\right)(1-\alpha_{iw})^n \quad (22)$$

where:

$$\exp\left(-\frac{E}{RT_w}\right) = \exp\left[-\frac{E}{R(T_c+\delta T)}\right] = \exp\left(-\frac{E}{RT_C}\frac{1}{1+\delta T/T_w}\right) \quad (23)$$

$$\exp\left(-\frac{E}{RT_w}\right) = \exp\left[-\frac{E}{RT_C}\left(1-\frac{\delta T}{T_C}\right)\right] \quad (24)$$

Bringing Eq. 18 and Eq. 24 into Eq. 23 gives:

$$[(1-\alpha_{iw})/(1-\alpha_{ic})]^n \exp(E\delta T/RT_C^2) = 1/2 \quad (25)$$

Therefore, the number of reaction levels n can be expressed as:

$$n = \frac{\ln(1/2)}{\delta T H_C/(1-\alpha_{ic}) + \ln[(1-\alpha_{iw})/(1-\alpha_{ic})]} \quad (26)$$

Bringing Eqs. 20 and 26 into Eq. 1 yields the finger front factor:

$$A = \beta H_c \exp(E/RT)(1-\alpha_{ic})^{-n} \quad (27)$$

After several iterations of calculation, the Gaussian multi-peak fitting formula is obtained:

$$y = y_0 + \frac{S}{w\sqrt{\pi/2}}\exp\left[-2\left(\frac{x-x_c}{w}\right)^2\right] \quad (28)$$

In Eq. 28, y_0 represents the baseline, S is the peak area, w is the half-height width of the peak, and x_c is the peak position.

Equations were used to obtain the reaction kinetic parameters for each pyrolysis stage. The kinetic parameters of pyrolysis for all films were collated in Table 5.

Table 5. Gaussian Multi-Peak Fitting Haircut to Determine the Fitting Parameters for Each Stage

Sample	Peak	X_c	w	S	H_c	n	E	R^2
No.1	1	290.90	40.77	0.70	0.01	6.90	118.16	0.933
	2	433.60	24.74	0.07	0.00	4.79	178.86	
No.2	1	300.71	67.92	0.69	0.01	14.69	149.97	0.978
	2	430.92	59.49	0.13	0.00	32.24	581.32	
No.3	1	292.14	43.86	0.78	0.01	3.20	59.07	0.995
	2	431.98	45.33	0.09	0.00	6.83	180.69	
No.4	1	299.21	50.64	0.73	0.01	3.32	51.28	0.990
	2	426.44	46.51	0.12	0.00	5.62	150.32	
No.5	1	300.13	53.77	0.72	0.01	2.88	38.61	0.990
	2	433.68	56.81	0.10	0.00	8.09	137.76	
No.6	1	300.70	55.37	0.64	0.01	13.53	156.82	0.991
	2	429.48	53.74	0.12	0.00	13.32	1402.72	

The Gaussian fit was considered effective, since the coefficients of determination were all greater than 0.95, except for the first film. However, the results of the apparent activation energies that were calculated were not satisfactory. The values of apparent activation energy of films in the range of 100 to 150 kJ/mol are considered normal, as suggested by the F-W-O and modified C-R methods. The appearance of 581 and 1402 kJ/mol in Table 5 was abnormal. Matching anomalous E values to n values, the n values showed a different change, *i.e.*, the E values deviated significantly when the n values became larger until they exceed 10. This deviation is unavoidable because, based on the exponential formula, the deviation is eventually reacted in terms of E-value. In other words, the abrupt change in n value implies a change in the thermal decomposition mechanism of the film. This change in mechanism affects the distribution of apparent activation energy. Comparing the analysis of the pyrolysis parameters of films No. 3, No. 4, and No. 5, a pattern was found. Although peak No.1 represents a greater rate of mass loss, it requires less energy. This phenomenon suggested that before 300 °C, about 50% of the mass loss requires only a small amount of energy, while more energy was used to support the remaining 35% mass loss (300 to 450 °C). The difference in energy required for the two peaks of the pure PVOH film was not significant, as suggested in Table 5. Although the content of NFCs and CQDs was small, it changed the thermal decomposition properties of the copolymer, which cannot be demonstrated by the "model-free" method.

To verify the accuracy of the results of fitting the reaction kinetic equations for each pyrolysis stage, the total conversions obtained by weighted superposition are presented. Total conversion rate is defined as follows,

$$\alpha = (S_1/\sum_{i=1}^{2} S_i)\alpha_1 + (S_2/\sum_{i=1}^{2} S_i)\alpha_2 \quad (29)$$

where S represents the integrated area of the single-step fitted peak curve. Each film fitting curve was collapsed in Fig. 7.

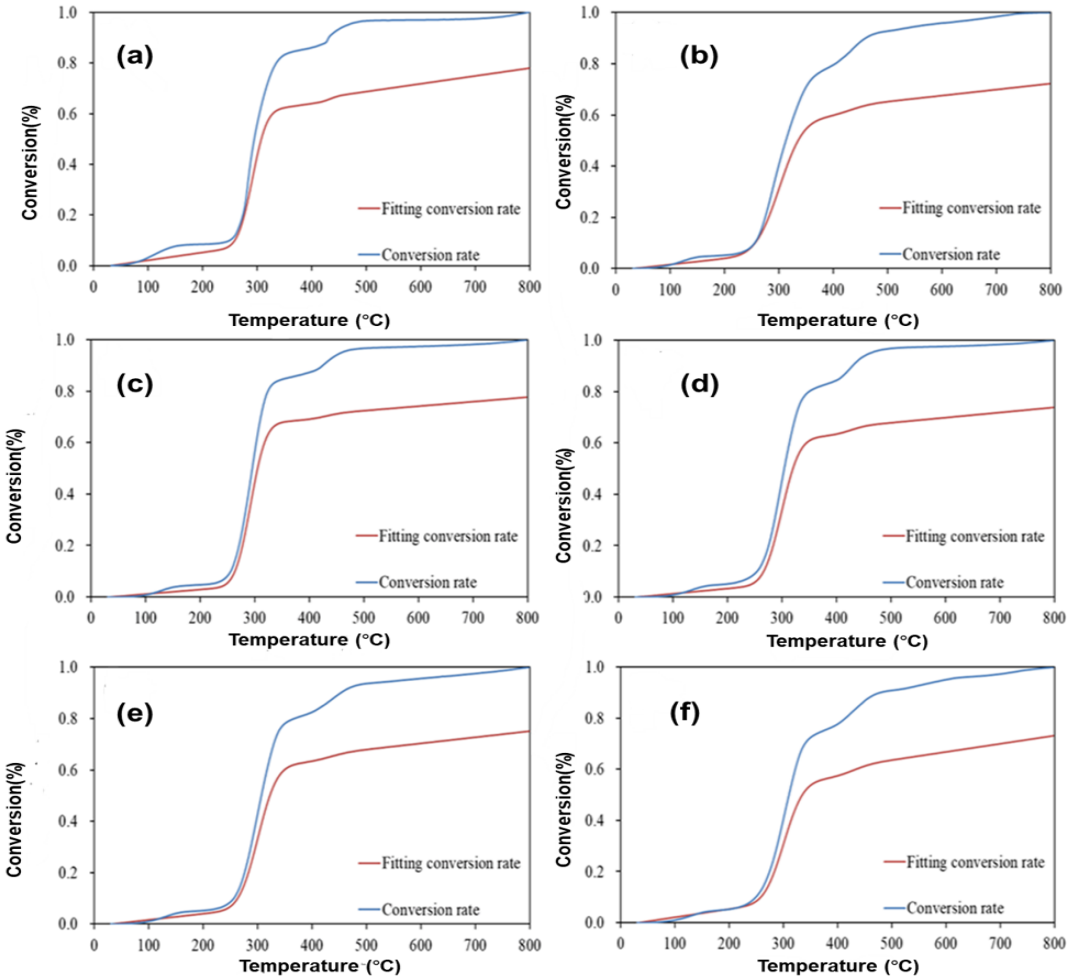

Fig. 7. Comparison of the fitted curve with the true curve. (a) film No. 1. (b) film No. 2. (c) film No. 3. (d) film No. 4. (e) film No. 5. (f) film No. 6

A noteworthy phenomenon emerged, where the curves in the range of 0 to 300 °C were considered as valid simulations. Above 300 °C, the simulated curves differ from the actual conversion curves. One possible explanation for the difference is that the degradation mechanism may change above 300 °C and the existing models do not simulate the whole process of pyrolysis. Different models of pyrolysis cooperate in order to investigate a more accurate process of pyrolysis.

Combination of PVOH and NFC

Considering the method of film preparation, it can be expected that the PVOH forms lamellar interlayers with NFC. These lamellar structures were plate-like. Further

structural predictions are collated in Fig. 8. Considering that the addition of NFC reduced the apparent activation energy of pure PVOH film, a possible explanation is that the hydrogen bonding of PVOH to the oxygen atoms of NFC limits the mobility of PVOH chains, which may lead to a reduction in the crystalline region of PVOH (Mansur *et al*. 2008). In other words, less initiation energy is required to support the decomposition of PVOH.

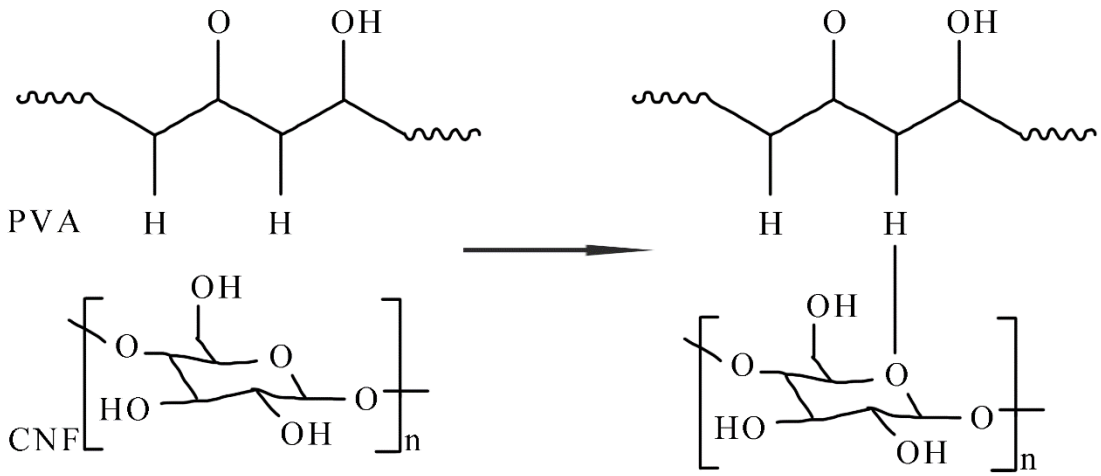

Fig. 8. Schematic diagram of the combination of PVOH and NFC

CONCLUSIONS

1. The mixture of nanofibrillated cellulose and carbon quantum dots (CQD) did not improve the apparent activation energy of the PVOH film, and even reduced it. The differential scanning calorimetry (DSC) tests supported this conclusion. The apparent activation energy of the pure poly(vinyl alcohol) PVOH film calculated with the F-W-O model was 149 kJ/mol, and the apparent activation energy of the film was improved by the addition of NFC and CQDs, ranging from 108 to 122 kJ/mol. The Gaussian fitting method confirms that the films change continuously and differently during thermal decomposition. The maximum activation energy was in the temperature range of 350-500 °C.
2. The results calculated by the modified C-R and Kissinger models were similar to those of the F-W-O model. The fit coefficient of the F-W-O model was the largest with the modified C-R model, which was 98.83 ± 0.80%.
3. The addition of NFC and CQD did not create a new chemical bond with PVOH. The PVOH was bound to NFC and CQD through hydrogen bonding.

ACKNOWLEDGMENTS

The authors acknowledge the support of the Advanced Analysis and Testing Center of Nanjing Forestry University.

Conflicts of Interest

There is no conflict of interest among authors.

Author Contributions

Yutong Wang designed the study and conducted parts of experiments and data analysis, Shiqi Xu-and Zhuangzhuang Teng wrote the initial manuscript.-Shiqi Xu revised the manuscript. Keke Liang performed the composite property testing/data analysis. All authors read and approved the manuscript.

REFERENCES CITED

Antal, M., Varhegyi, G., and Jakab, E. (1998). "Cellulose pyrolysis kinetics: The current state of knowledge," *Industrial and Engineering Chemistry Research* 37, 1267-1277.

Baker, S. N., and Baker, G. A. (2011). "ChemInform abstract: Luminescent carbon nanodots: Emergent nanolights," *ChemInform* 42(3).

Bersanetti, P. A., Escobar, V. H., Nogueira, R. F., Ortega, F. d. S., Schor, P., and Morandim-Giannetti, A. d. A. (2019). "Enzymatically obtaining hydrogels of PVOH crosslinked with ferulic acid in the presence of laccase for biomedical applications," *European Polymer Journal* 112, 610-618. https://doi.org/10.1016/j.eurpolymj.2018.10.024

Bottini, M. , Balasubramanian, C., Dawson, M. I., Bergamaschi, A., Bellucci, S., and Mustelin, T.. (2006). "Isolation and characterization of fluorescent nanoparticles from pristine and oxidized electric arc-produced single-walled carbon nanotubes," *Journal of Physical Chemistry B* 110(2), 831-6. https://doi.org/10.1021/jp055503b

Brown, M. E., Maciejewski, M., Vyazovkin, S., Nomen, R., and Janssens, J. (2000). "Computational aspects of kinetic analysis," *Thermochimica Acta* 355(1), 155-163.

Cai, J. M., Xu, D., Dong, Z. J., Yu, X., Yang, Y., Banks, S. W., and Bridgwater, A. V. (2018). "Processing thermogravimetric analysis data for isoconversional kinetic analysis of lignocellulosic biomass pyrolysis: Case study of corn stalk," *Renewable and Sustainable Energy Reviews* 82, 2705-2715. https://doi.org/10.1016/j.rser.2017.09.113

Chen, C. C., and Fan, T. (2017). "Study on carbon quantum dots/BiFeO3 heterostructures and their enhanced photocatalytic activities under visible light irradiation," *Journal of Materials Science-Materials in Electronics* 28(14), 10019-10027. https://doi.org/10.1007/s10854-017-6760-6

Conesa, J. A., Caballero, J., Marcilla, A., and Font, R. (1995). "Analysis of different kinetic models in the dynamic pyrolysis of cellulose," *Thermochimica Acta* 254, 175-192. https://doi.org/10.1016/0040-6031(94)02102-T

Cui, S. Y., Wei, P. F., and Li, L. (2019). "Thermal decomposition behavior of poly(propylene carbonate) in poly(propylene carbonate)/poly(vinyl alcohol) blend," *Journal of Thermal Analysis and Calorimetry* 135(4), 2437-2446. https://doi.org/10.1007/s10973-018-7297-5

Ding, H., Yu, S. B., Wei, J. S., and Xiong, H. M. (2016). "Full-color light-emitting carbon dots with a surface-state-controlled luminescence mechanism," *ACS Nano* 10(1), 484-491.

dos Santos, G. D., dos Santos, N. R. R., Pereira, I. C. S., de Andrade, A. J., Lima, E. M. B., Minguita, A. P., Rosado, L. H. G., Duarte Moreira, A. P., Middea, A., Prudencio,

E. R., Luchese, R. H., and Oliveira, R. N. (2020). "Layered cryogels laden with Brazilian honey intended for wound care," *Polimeros-Ciencia E Tecnologia* 30(3). https://doi.org/10.1590/0104-1428.06820

Dufresne, A. (2013). "Nanocellulose: A new ageless bionanomaterial," *Materials Today* 16(6), 220-227.

El-Shamy, A. G. (2019). "Novel conducting PVOH/Carbon quantum dots (CQDs) nanocomposite for high anti-electromagnetic wave performance," *Journal of Alloys and Compounds* 810. https://doi.org/10.1016/j.jallcom.2019.151940

Evans, R. J., and Milne, T. A. (1987). "Molecular characterization of the pyrolysis of biomass," *Energy Fuel* 1(2), article e25514.

Flynn, J. H., and Wall, L. A. (1966). "General treatment of the thermogravimetry of polymers," *Journal of Research of the National Bureau of Standards–A. Physics and Chemistry* 70*A*(6).

Friedman, H. L. (1964). "Kinetics of thermal degradation of char-forming plastics from thermogravimetry. Application to a phenolic plastic," *Journal of Polymer Science Part C: Polymer Symposia* 6(1).

Garrett, L. G., Smaill, S. J., Beets, P. N., Kimberley, M. O., and Clinton, P. W. (2021). "Impacts of forest harvest removal and fertiliser additions on end of rotation biomass, carbon and nutrient stocks of *Pinus radiata*," *Forest Ecology and Management* 493. https://doi.org/10.1016/j.foreco.2021.119161

Guo, Y., Zhang, L., Zhang, S., Yang, Y., Chen, X., and Zhang, M. (2015). "Fluorescent carbon nanoparticles for the fluorescent detection of metal ions," *Biosensors and Bioelectronics* 63, 61-71.

Guo, Z. Y., Wang, Q., Shen, T., Hou, X. J., Kuang, J. L., Liu, W. X., and Cao, W. B. (2019). "Synthesis of 3D CQDs/urchin-like and yolk-shell TiO_2 hierarchical structure with enhanced photocatalytic properties," *Ceramics International* 45(5), 5858-5865. https://doi.org/10.1016/j.ceramint.2018.12.052

Hao, X. L., Huang, L. L., Zhao, C. F., Chen, S. N., Lin, W. J., Lin, Y. N., Zhang, L., Sun, A., Miao, C. F., Lin, X. H., Chen, M., and Weng, S. H. (2021). "Antibacterial activity of positively charged carbon quantum dots without detectable resistance for wound healing with mixed bacteria infection," *Materials Science and Engineering C-Materials for Biological Applications* 123, article 111971. https://doi.org/10.1016/j.msec.2021.111971

Jiang, F., and Hsieh, Y. L. (2016). "Self-assembling of TEMPO oxidized cellulose nanofibrils as affected by protonation of surface carboxyls and drying methods," *ACS Sustainable Chemistry and Engineering* 4(3), 1041-1049. https://doi.org/10.1021/acssuschemeng.5b01123

Kissinger, H. E. (1956). "Variation of peak temperature with heating rate in differential thermal analysis," *Journal of Research of the National Bureau of Standards* 57(4), 217-221.

Klemm, D., Kramer, F., Moritz, S., Lindström, T., Ankerfors, M., and Gray, D., and Dorris, A. (2010). "Nanocelluloses: A new family of nature-based materials," *Angewandte Chemie International Edition* 50(24), 5438-5466. https://doi.org/10.1002/anie.201001273

Kong, B., Zhu, A., Ding, C., Zhao, X., Li, B., and Tian, Y. (2012). "Carbon dot-based inorganic-organic nanosystem for two-photon imaging and biosensing of pH variation in living cells and tissues," *Advanced Materials* 24(43), 5844-5848.

Koverzanova, E. V., Usachev, S. V., Lomakin, S. M., Shilkina, N. G., Shaulov, A. Y., and

Berlin, A. A. (2019). "Kinetics of the thermal destruction of polyvinyl alcohol in composites with boron polyoxide. Part 2. Analysis of the products of thermal destruction," *Russian Journal of Physical Chemistry B* 13(3), 514-518. https://doi.org/10.1134/s1990793119030060

Li, H., Zhang, Y., Wang, L., Tian, J., and Sun, X. (2010). "Nucleic acid detection using carbon nanoparticles as a fluorescent sensing platform," *Chemical Communications* 47(3), 961-963.

Li, W., Yue, J. Q., and Liu, S. X. (2012). "Preparation of nanocrystalline cellulose via ultrasound and its reinforcement capability for poly(vinyl alcohol) composites," *Ultrasonics Sonochemistry* 19(3), 479-485. https://doi.org/10.1016/j.ultsonch.2011.11.007

Limpan, N., Prodpran, T., Benjakul, S., and Prasarpran, S. (2012). "Influences of degree of hydrolysis and molecular weight of poly(vinyl alcohol) (PVOH) on properties of fish myofibrillar protein/PVOH blend films," *Food Hydrocolloids* 29(1), 226-233. https://doi.org/10.1016/j.foodhyd.2012.03.007

Lin, J. X., Song, Y., Xie, Z. H., Guo, Y. C., Yuan, B., Zeng, J. J., and Wei, X. (2020). "Static and dynamic mechanical behavior of engineered cementitious composites with PP and PVOH fibers," *Journal of Building Engineering* 29. https://doi.org/10.1016/j.jobe.2019.101097

Liu, B., Qiu, D., and Chunzhen, Z. (2010). "Effect of mixture of plasticizer on the thermoplastics formability of polyvinyl alcohol (PVOH)," *Key Engineering Materials* 447-448, 652-656.

Lu, J., Wang, T., and Drzal, L. T. (2008). "Preparation and properties of microfibrillated cellulose polyvinyl alcohol composite materials," *Composites Part A – Applied Science and Manufacturing* 39(5), 738-746. https://doi.org/10.1016/j.compositesa.2008.02.003

Mansur, H. S., Sadahira, C. M., Souza, A. N., and Mansur, A. A. P. (2008). "FTIR spectroscopy characterization of poly (vinyl alcohol) hydrogel with different hydrolysis degree and chemically crosslinked with glutaraldehyde," *Materials Science and Engineering C-Biomimetic and Supramolecular Systems* 28(4), 539-548. https://doi.org/10.1016/j.msec.2007.10.088

Marini, A., Berbenni, V., and Flor, G. (1979). "Kinetic parameters from thermogravimetric data," *Zeitschrift Für Naturforschung A* 34(5).

Mashkour, M., Kimura, T., Kimura, F., Mashkour, M., and Tajvidi, M. (2014). "Tunable self-assembly of cellulose nanowhiskers and polyvinyl alcohol chains induced by surface tension torque," *Biomacromolecules* 15(1), 60-65. https://doi.org/10.1021/bm401287s

Mehta, A., Pooja, D., Thakur, A., and Basu, S. (2017). "Enhanced photocatalytic water splitting by gold carbon dot core shell nanocatalyst under visible/sunlight," *New Journal of Chemistry* 41(11), 4573-4581. https://doi.org/10.1039/c7nj00933j

Morán, J., Alvarez, V. A., Cyras, V. P., and Vázquez, A. (2008). "Extraction of cellulose and preparation of nanocellulose from sisal fibers," *Cellulose* 15(1), 149-159.

Ozawa, and Takeo. (1965). "A new method of analyzing thermogravimetric data," *Bull.chem.soc.jpn,* 38(11), 1881-1886.

Patchiya, P., Prasert, R., Hao, X., Xu, G., Abuliti, A., and Guan, G. (2018). "Nanocellulose: Extraction and application," *Carbon Resources Conversion* S2588913318300036-.

Pei, S., Zhang, J., Gao, M., Wu, D., and Liu, R. (2015). "A facile hydrothermal approach

towards photoluminescent carbon dots from amino acids," *Journal of Colloid and Interface Science* 439, 129-133.

Qua, E. H., Hornsby, P. R., Sharma, H. S. S., Lyons, G., and McCall, R. D. (2009). "Preparation and characterization of poly(vinyl alcohol) nanocomposites made from cellulose nanofibers," *Journal of Applied Polymer Science* 113(4), 2238-2247. https://doi.org/10.1002/app.30116

Sarma, S., Mothudi, B. M., Dhlamini, M. S., and Ray, S. C. (2018). "Conduction mechanisms in polyvinyl alcohol: CdS/CdS:Cu nanoparticle hybrid nanocomposites," *Journal of Nanoscience and Nanotechnology* 18(2), 1369-1375. https://doi.org/10.1166/jnn.2018.15208

Shafizadeh, F. (1982). "Introduction to pyrolysis of biomass," *Journal of Analytical and Applied Pyrolysis* 3(4), 283-305.

Shafizadeh, F. (1985). *Pyrolytic Reactions and Products of Biomass*, Springer Netherlands.

Shin, W. J., Won, T., and Lee, C. S. (2007). "Multi-domain PVOH LCD cell: Pros and cons," *Molecular Crystals and Liquid Crystals* 476, 433-441. https://doi.org/10.1080/15421400701686926

Silverio, H. A., Neto, W. P. F., and Pasquini, D. (2013). "Effect of incorporating cellulose nanocrystals from corncob on the tensile, thermal and barrier properties of poly(vinyl alcohol) nanocomposites," *Journal of Nanomaterials* 2013. https://doi.org/10.1155/2013/289641

Sin, L. T., Rahman, W., Rahmat, A. R., and Mokhtar, M. (2011). "Determination of thermal stability and activation energy of polyvinyl alcohol-cassava starch blends," *Carbohydrate Polymers* 83(1), 303-305. https://doi.org/10.1016/j.carbpol.2010.07.049

Bottini, M. , Balasubramanian, C., Dawson, M. I., Bergamaschi, A., Bellucci, S., and Mustelin, T. (2006). "Isolation and characterization of fluorescent nanoparticles from pristine and oxidized electric arc-produced single-walled carbon nanotubes," *Journal of Physical Chemistry B* 110(2), 831-836. https://doi.org/10.1021/jp055503b

Stankovich, S., Dikin, D. A., Dommett, G. H. B., Kohlhaas, K. M., Zimney, E. J., Stach, E. A., Piner, R. D., Nguyen, S. B. T., and Ruoff, R. S. (2006). "Graphene-based composite materials," *Nature* 442(7100), 282-286. https://doi.org/10.1038/nature04969

Sun, Y. P., Zhou, B., Lin, Y., Wang, W., and Fernando, K. (2006). "Quantum-sized carbon dots for bright and colorful photoluminescence," *Journal of the American Chemical Society* 128(24), 7756-7757. https://doi.org/10.1021/ja062677d

Takahashi, Y., Fujita, H., and Sakoda, A. (2014). "Functions of amorphous carbon in catalyst fabrication for carbon nanofiber growth in the poly(ethylene glycol) thermal decomposition method," *Journal of Materials Science* 49(15), 5289-5298. https://doi.org/10.1007/s10853-014-8231-2

Tang, X. Z., and Alavi, S. (2011). "Recent advances in starch, polyvinyl alcohol based polymer blends, nanocomposites and their biodegradability," *Carbohydrate Polymers* 85(1), 7-16. https://doi.org/10.1016/j.carbpol.2011.01.030

Thomas, P. S., Guerbois, J. P., Russell, G. F., and Briscoe, B. J. (2001). "FTIR study of the thermal degradation of poly(vinyl alcohol)," *Journal of Thermal Analysis and Calorimetry* 64(2), 501-508. https://doi.org/10.1023/a:1011578514047

Tian, H., Zhang, Y. X., Yang, C. H., and Ding, Y. N. (2016). "Recent advances in experimental studies of the mechanical behaviour of natural fibre-reinforced

cementitious composites," *Structural Concrete* 17(4), 564-575. https://doi.org/10.1002/suco.201500177

Voronova, M. I., Surov, O. V., Guseinov, S. S., Barannikov, V. P., and Zakharov, A. G. (2015). "Thermal stability of polyvinyl alcohol/nanocrystalline cellulose composites," *Carbohydrate Polymers* 130, 440-447. https://doi.org/10.1016/j.carbpol.2015.05.032

Wang, H., Wu, T., Wang, X., Cheng, X., and Li, D. (2019). "Effect of ethylenediamine treatment on cellulose nanofibers and the formation of high-strength hydrogels," *BioResources* 14(1), 1141-1156. https://doi.org/10.15376/biores.14.1.1141-1156

Wang, X., Bian, H. Y., Ni, S. Z., Sun, S. R., Jiao, L., and Dai, H. Q. (2020). "BNNS/PVOH bilayer composite film with multiple-improved properties by the synergistic actions of cellulose nanofibrils and lignin nanoparticles," *International Journal of Biological Macromolecules* 157, 259-266. https://doi.org/10.1016/j.ijbiomac.2020.04.178

Wang, Y., Zhuang, Q. F., and Ni, Y. N. (2015). "Facile microwave-assisted solid-phase synthesis of highly fluorescent nitrogen-sulfur-codoped carbon quantum dots for cellular imaging applications," *Chemistry-a European Journal* 21(37), 13004-13011. https://doi.org/10.1002/chem.201501723

Xu, L., Zhang, Y., Pan, H., Xu, N., and Xu, C. (2019). "Preparation and Performance of radiata-pine-derived polyvinyl alcohol/carbon quantum dots fluorescent films," *Materials* 13(1), 67.

Xu, X. Y., Ray, R., Gu, Y. L., Ploehn, H. J., Gearheart, L., Raker, K., and Scrivens, W. A. (2004). "Electrophoretic analysis and purification of fluorescent single-walled carbon nanotube fragments," *Journal of the American Chemical Society* 126(40), 12736-12737. https://doi.org/ 10.1021/ja040082h

Yang, F., Li, J., Long, Y., Zhang, Z., Wang, L., Sui, J., Dong, Y., Wang, Y., Taylor, R., Ni, D., Cai, W., Wang, P., Hacker, T., and Wang, X. (2021). "Wafer-scale heterostructured piezoelectric bio-organic thin films," *Science* 373(6552), 337-342. https://doi.org/10.1126/science.abf2155

Yao, F., Wu, Q. L., Lei, Y., Guo, W. H., and Xu, Y. J. (2008). "Thermal decomposition kinetics of natural fibers: Activation energy with dynamic thermogravimetric analysis," *Polymer Degradation and Stability* 93(1), 90-98. https://doi.org/10.1016/j.polymdegradstab.2007.10.012

Yao, F., Wu, Q., Lei, Y., Guo, W., and Xu, Y. (2008). "Thermal decomposition kinetics of natural fibers: Activation energy with dynamic thermogravimetric analysis," *Polymer Degradation and Stability* 93(1), 90-98. https://doi.org/10.1016/j.polymdegradstab.2007.10.012

Yeum, J. H., Kwak, J. W., Han, S. S., Kim, S. S., Ji, B. C., Noh, S. K., and Lyoo, W. S. (2004). "Water stability of high-molecular-weight (HMW) syndiotacticity-rich poly(vinyl alcohol) (PVOH)/HMW atactic PVOH/iodine complex blend films," *Journal of Applied Polymer Science* 94(4), 1435-1439. https://doi.org/10.1002/app.21048

Zhang, B., Liu, C. Y., and Yun, L. (2010). "A novel one-step approach to synthesize fluorescent carbon nanoparticles," *European Journal of Inorganic Chemistry* 2010(28), 4411-4414.

Zhang, L. J., Ye, D. Z., Tang, J. B., Hu, X. Q., and Zhang, X. (2016). "Interaction of lignosulfonate calcium and polyvinyl alcohol and the performance of the blending material," *Acta Polymerica Sinica* (4), 471-476.

Zhang, W., He, X., Li, C. Y., Zhang, X. X., Lu, C. H., Zhang, X. D., and Deng, Y. L.

(2014). "High performance poly (vinyl alcohol)/cellulose nanocrystals nanocomposites manufactured by injection molding," *Cellulose* 21(1), 485-494. https://doi.org/10.1007/s10570-013-0141-y

Zhou, J., Booker, C., Li, R., Zhou, X., Sham, T. K., Sun, X., and Ding, Z. (2007). "An electrochemical avenue to blue luminescent nanocrystals from multiwalled carbon nanotubes (MWCNTs)," *Journal of the American Chemical Society* 129(4), 744-745.

Article submitted: February 27, 2024; Peer review completed: April 12, 2024; Revised version received: May 6, 2024; Accepted: May 7, 2024; Published: April 17, 2026.
DOI: 10.15376/biores.21.2.4872-4898